Hindawi
Advances in Civil Engineering
Volume 2020, Article ID 4961963, 16 pages
https://doi.org/10.1155/2020/4961963

Research Article

Integrating the Finite Element Method with a Data-Driven Approach for Dam Displacement Prediction

Chenfei Shao,[1,2] Chongshi Gu,[1,2] Zhenzhu Meng,[3] and Yating Hu[1,2,3]

[1]*College of Water Conservancy and Hydropower Engineering, Hohai University, Nanjing 210098, China*
[2]*National Engineering Research Center of Water Resources Efficient Utilization and Engineering Safety, Nanjing 210098, China*
[3]*Laboratory of Environmental Hydraulics, École Polytechnique Fédérale de Lausanne, 1015 Lausanne, Switzerland*

Correspondence should be addressed to Chongshi Gu; csgu@hhu.edu.cn

Received 24 September 2019; Revised 6 December 2019; Accepted 17 February 2020; Published 22 April 2020

Academic Editor: Luigi Di Sarno

Both numerical simulations and data-driven methods have been applied in dam's displacement modeling. For monitored displacement data-driven methods, the physical mechanism and structural correlations were rarely discussed. In order to take the spatial and temporal correlations among all monitoring points into account, we took the first step toward integrating the finite element method into a data-driven model. As the data-driven method, we selected the random coefficient model, which can make each explanatory variable coefficient of all monitoring points following one or several normal distributions. In this way, explanatory variables are constrained. Another contribution of the proposed model is that the actual elastic modulus at each monitoring point can be back-calculated. Moreover, with a Lagrange polynomial interpolation, we can obtain the distribution field of elastic modulus, rather than gaining one value for the whole dam in previous studies. The proposed model was validated by a case study of the concrete arch dam in Jinping-I hydropower station. It has a better prediction precision than the random coefficient model without the finite element method.

1. Introduction

For dams that have been running for years, their actual physical and mechanical properties often have considerable differences from the initial or design values, due to the effect of external environment. Hence, it is crucial to monitor and evaluate the dam's structural behaviors and its actual material properties. Using monitoring devices installed inside the dam, displacement, rotation, seepage, and stress can be measured, among which displacement is the most important [1]. Dam's displacement is not only affected by the external conditions (e.g., water load, temperature, and aging), but also depends on its material properties such as elastic modulus. Elastic modulus, the ratio of applied external stress to the elastic deformation of material, is usually difficult to measure; hence, it is often obtained by back-analysis based on monitored displacement data.

For the dam's displacement prediction, two approaches have been commonly used: one is numerical simulation using finite element method [2, 3]; another is data-driven method based on monitored displacement data [4, 5]. The principle of numerical simulations is to solve the constitutive equations; emphasis is given on physical mechanism governing the displacement [6, 7]. Yet the numerical simulation often has considerable inaccuracies induced by unavoidable simplifications and idealizations of the dam's structural and material properties. Moreover, the simulation results fully depend on the initial setting of parameters, without any calibration with the actual displacement. Many researches have improved the accuracy of finite element method, especially when complex situations are involved [8–10]. However, there is still a gap in integrating the numerical simulation with monitored data in real world and avoiding the inaccuracies due to structural simplifications.

For data-driven methods, with the development of soft computing techniques, the modeling algorithms improved from the simple linear regression methods [11–13] to the advanced machine learning methods such as support vector

machines (SVM) [14, 15] and artificial neural network (ANN) [16]. In recent years, many synthetic models that integrate several machine learning methods also have been carried out [17, 18]. Unlike the finite element methods that simulate the dam's behavior based on the design structural and material properties, data-driven methods cope with monitored data in real world. However, compared with the fact that finite element method can simulate the displacement of arbitrary point on the dam, the statistical model can merely model the displacement at the monitoring point. In addition, the data recorded at each monitoring point were modeled independently; the spatial and temporal correlations among the monitoring points were rarely discussed, which may weaken the generalization ability and sometimes result in overfitting problems [19, 20].

In order to take considerations of spatial correlations among monitoring points in data-driven models, recent researches integrated clustering models with statistical models; they first clustered the monitoring points into several groups based on one or several indicators and then constrained the coefficients of explanatory variables in statistical model based on the clustering results. Shao et al. clustered the monitoring points based on their spatial characteristics, namely, distance from the monitoring point to the dam foundation [21]. Hu et al. provided a clustering model that considers the temporal-spatial characteristics [22]. However, their constraint ability is still not satisfactory, as they provided constraint for each group rather than for each monitoring point. The primary objective of the present study is to consider spatial correlations and provide constraints for each monitoring point rather than for each group.

With this objective in mind, we took advantage of finite element method that can simulate the deformation at any arbitrary point on the dam to consider the structural correlations of each monitoring point. Specifically, we determined that the water pressure component and temperature component of the whole region of dam with the finite element model, the ratio of design and actual elastic modulus, and the ratio of design and actual coefficient of linear expansion are only variables in the proposed model. Then we constructed variables relating to time in aging component to consider the temporal correlations. The random coefficient model assumes the monitoring points as a panel and the coefficients of all explanatory variables in the model following a Gaussian distribution, which constrains the coefficients at a certain extent. The multicollinearity problem is solved by constraining the explanatory variables and the model becomes more stable and has a better prediction ability. Another contribution of the proposed model is that the actual elastic modulus can be back-calculated for each monitoring point. Rather than gaining one elastic modulus for the whole dam in previous studies, with a Lagrange polynomial interpolation, we obtained a distribution field of elastic modulus from the value at each monitoring point.

This article is organized as follows. Section 2 presents the development of the synthetic model that combines the finite element method with the random coefficient model. The engineering project and dataset are exhibited in Section 3. The modeling results are presented in Section 4. Section 5 discusses the prediction precision of the proposed model and the distribution field of elastic modulus. Concluding remarks complete the paper in Section 6.

2. Methods

2.1. Statistical Model. In the statistical model, the concrete dam's displacement δ is commonly divided into three components: the water pressure component δ_H, the temperature component δ_T, and the aging component δ_θ [23]. The dam's displacement is expressed as follows:

$$\delta = \delta_H + \delta_\theta + \delta_T. \tag{1}$$

2.1.1. Water Pressure Component. The water pressure component δ_H includes displacement caused by itself δ_{1H}, dam foundation δ_{2H}, and rotation of the dam bedrock δ_{3H}, which are made up of polynomials of H, H^2, H^3, H^4 [1]. δ_H can be simplified as

$$\delta_H = \sum_{i=1}^{n} a_i H^i, \tag{2}$$

where H is the upstream water level, a_i are the coefficients of water pressure component which are related to the dam height h, m is the downstream slope angle, and d is the distance from the monitoring point to the dam foundation, which are constants for indicated monitoring points. In addition, a_i also depends on dam's material properties including elastic modulus of the dam body E_c, Poisson's ratio of the dam body μ_c, elastic modulus of the foundation E_r, and Poisson's ratio of the foundation μ_r. Poisson's ratios μ_c and μ_r have negligible effect on the dam's displacement. Therefore, the elastic modulus of the dam body and elastic modulus of the foundation E_c and E_r are the merely random coefficients in the water pressure component.

2.1.2. Temperature Component. The temperature component δ_T is mainly composed of the displacement produced by the temperature variation of dam body concrete and dam foundation rock. When there is lack of temperature data, multiperiod harmonic is used to describe the temperature component:

$$\delta_T = \sum_{i=1}^{m_3} \left(b_{1i} \sin \frac{2\pi i t}{365} + b_{2i} \cos \frac{2\pi i t}{365} \right), \tag{3}$$

where i indicates the period; for the annual cycle $i = 1$, and for half a cycle $i = 2$; b_{1i} and b_{2i} represent coefficients; t is the cumulative number of days from the initial value to monitoring value; and m_3 is usually taken as 1 or 2.

2.1.3. Aging Component. Under long-term external loads, the dam produces inelastic displacement related to time; a fixed form of trend function is used to describe the aging component:

$$\delta_\theta = c_1\theta + \ln\theta, \tag{4}$$

where $\theta = (t/100)$.

In summary, according to the characteristics of concrete dam, the statistical model of concrete dam can be depicted as

$$\delta = a_0 + \sum_{i=1}^{n} a_i H^i + \sum_{i=1}^{m_3}\left(b_{1i}\sin\frac{2\pi it}{365} + b_{2i}\cos\frac{2\pi it}{365}\right) + c_1\theta + \ln\theta, \tag{5}$$

where a_0 denotes the constant term; other symbols mean the same as above.

2.2. Combination of the Finite Element Method and Statistical Model. In the proposed model, we can obtain simulated water pressure component and temperature component by the finite element method with design material parameters. The actual elastic modulus of the dam body E_c and actual elastic modulus of the dam foundation E_r can be expressed as $E_r = \lambda E_c$; then, δ_H becomes

$$\delta_H = \frac{1}{E_c}\sum_{i=1}^{n} a_i^0 H^i, \tag{6}$$

where a_i^0 are the coefficients determined by h, m, d, and λ. As expressed in equation (7), with a given design elastic modulus of the dam body E_c^0 and upstream water level H, we can obtain a numerical solution of water pressure component δ_H^0 using the finite element method. Then, we can obtain a series of coefficients a_i^1 by fitting the upstream water level H and numerical solution δ_H^0:

$$\delta_H^0 = \frac{1}{E_c^0}\sum_{i=1}^{n} a_i^1 H^i. \tag{7}$$

We then apply a_i^1 instead of a_i^0 to equation (6); the displacement component δ_H can be expressed as

$$\delta_H = \frac{E_c^0}{E_c}\frac{1}{E_c^0}\sum_{i=1}^{n} a_i^1 H^i = \frac{E_c^0}{E_c}\delta_H^0 = \xi\delta_H^0, \tag{8}$$

where ξ is the ratio from the design elastic modulus of the dam body E_c^0 to the actual elastic modulus of the dam body E_c.

Similar to δ_H, the coefficients of explanatory variables in the temperature component δ_T can also be determined using the finite element method. The displacement depending on temperature load in one dimension can be described by $\mathrm{d}L = \alpha L \mathrm{d}T$, where α is the coefficient of linear expansion, L is the length, and T is temperature. The coefficient of linear expansion α_c can be considered as the only random coefficient. The temperature component δ_T can be expressed as

$$\delta_T = \alpha_c \sum_{i=1}^{n} b_i^0 T^i, \tag{9}$$

where b_i^0 represents the coefficients of temperature component, α_c is the actual coefficient of linear expansion of the dam body, and T is the environmental temperature. With a given design coefficient of linear expansion α_c^0 and temperature T, we can obtain a numerical solution of temperature component δ_T^0 using finite element method. By fitting the temperature T and the numerical solution δ_T^0, the coefficients b_i^1 of T can be obtained as

$$\delta_T^0 = \sum_{i=1}^{n} b_i^1 T^i. \tag{10}$$

We then apply b_i^1 instead of b_i^0 in equation (9), and δ_H then can be expressed as

$$\delta_T = \frac{\alpha_c}{\alpha_c^0}\frac{\alpha_c^0}{1}\sum_{i=1}^{n} b_i^1 T^i = \frac{\alpha_c}{\alpha_c^0}\delta_T^0 = \psi\delta_T^0, \tag{11}$$

where ψ is the ratio from the actual coefficient of linear expansion α_c to design coefficient of linear expansion α_c^0.

The aging component δ_θ characterizes irreversible displacement caused by factors such as creep and fatigue of concrete. Due to the difficulties of expressing δ_θ theoretically, here, we provide a formula, which includes time and monitoring point's coordinates as variables, to describe its tendency:

$$\delta_\theta = \sum_{l=0}^{L}\sum_{m=0}^{M}(d_{1lm}\theta + d_{2lm}\ln\theta)x^l z^m, \tag{12}$$

where x is the horizontal coordinate and z is the vertical coordinate of the monitoring point, $\theta = (t/100)$, t is the cumulative number of days from the initial value to monitoring value, and d_{1lm} and d_{2lm} are unknown coefficients. Then, the radial displacement can be exhibited as

$$\begin{aligned}\delta_i &= \delta_{iH} + \delta_{iT} + \delta_{i\theta},\\ &= \xi_i\delta_H^0 + \psi_i\delta_T^0 + \sum_{l=0}^{L}\sum_{m=0}^{M}(d_{1lm}\theta + d_{2lm}\ln\theta)x_i^l z_i^m + u,\end{aligned} \tag{13}$$

where i is the index of measuring point, u is the random error term, δ_H^0 are series of water pressure component calculated under groups of upstream water level H with finite element method, δ_T^0 are series of temperature component calculated under groups of temperature T with finite element method, and coefficients ξ_i, ψ_i, d_{1lm}, d_{2lm}, and u are unknown coefficients in the model of all monitoring points which can be calculated with random coefficient model.

In the model, we can obtain the actual material parameters E_c and ψ when ξ and ψ are calculated. In addition, $\xi_i\delta_H^0$ and $\psi_i\delta_T^0$ represent the displacement produced by water pressure and fluctuation of temperature; $\sum_{l=0}^{L}\sum_{m=0}^{M}(d_{1lm}\theta + d_{2lm}\ln\theta)x_i^l z_i^m$ represents the displacement produced owing to aging behavior of material such as creep and deterioration of material strength and so forth.

2.3. Solving with the Random Coefficient Model. With random coefficient model, pending coefficients in equation (9) of all monitoring points can be calculated simultaneously obeying an asymptotic normal distribution. The monitoring displacement data are two-dimensional panel data containing time series and cross-section panel. Data on one panel represent the displacement data at an indicated time.

The regression coefficients of one panel can be expressed by the following formula:

$$y_{it} = \sum_{k=1}^{K} \beta_{ki} x_{kit} + u_{it} = \sum_{k=1}^{K} (\beta_k + \gamma_{ki}) x_{kit} + u, \tag{14}$$

where y_{it} represents the two-dimensional dam displacement data; x_{kit} represents the two-dimensional data of explanatory variables; t is the time index; i is the index of section; k is the index of the explanatory variables; the coefficient β_{ki} is independent with time, which can be decomposed into β_k and γ_{ki}; $\beta = (\beta_1, \ldots, \beta_K)'$ is the common mean coefficient vector; $\gamma = (\gamma_{1i}, \ldots, \gamma_{Ki})'$ is the degree of the individual deviated from the common mean; u is the random error term.

The objective is to obtain β_{ki} from the two-dimensional data series y_{it} and x_{kit}. According to the above analysis, we consider that the random coefficients β_{ki} obey an asymptotic normal distribution. Here, $\beta_i = \beta + \gamma_i$ is considered as a random coefficient with a common mean value β; Swamy gave the following assumptions [24]. In the equations below, the symbol at the upper right corner of the letter represents the transposition operation:

$$\begin{aligned} E(\gamma_i \gamma_j') &= \begin{cases} \Delta, & i = j, \\ 0, & i \neq j. \end{cases} \\ E(\gamma_i) &= 0, \\ E(x_{it} \gamma_j') &= 0, \\ E(u_i u_j') &= \begin{cases} \sigma_i^2 I_T, & i = j, \\ 0, & i \neq j. \end{cases} \end{aligned} \tag{15}$$

By integrating the observation data, the matrix equation can be obtained as follows:

$$y = X\beta + \widetilde{X}\gamma + u, \tag{16}$$

where

$$\begin{aligned} y_{NT\times 1} &= (y_1', \ldots, y_N'), \\ X_{NT\times 1} &= \begin{bmatrix} X_1 \\ X_2 \\ \vdots \\ X_N \end{bmatrix}, \\ \widetilde{X}_{NT\times NK} &= \begin{pmatrix} X_1 & \cdots & 0 \\ \vdots & \ddots & \vdots \\ 0 & \cdots & X_N \end{pmatrix}, \\ u &= (u_1', \ldots, u_N')', \\ \gamma &= (\gamma_1', \ldots, \gamma_N')', \end{aligned} \tag{17}$$

where N is the number of panels, T is the amount of data in the panel, the compound error term $\widetilde{X}\gamma + u$ is a diagonal matrix, and the i-th diagonal block is $\psi_i = X_i \Delta X_i' + \sigma_i^2 I_T$. Under Swamy's assumption, the estimator of β using the ordinary least squares is biased. When $X'X/NT$ converges to a nonzero constant matrix, we can get a consistent noneffective estimation. The generalized least squares estimation $\widehat{\beta}_{\mathrm{GLS}}$ is the optimal linear unbiased estimator of β:

$$\begin{aligned} \widehat{\beta}_{\mathrm{GLS}} &= \left(\sum_{i=1}^{N} X_i' \psi_i^{-1} X_i \right)^{-1} \left(\sum_{i=1}^{N} X_i' \psi_i^{-1} y_i \right) = \sum_{i=1}^{N} W_i \widehat{\beta}_i, \\ W_i &= \left\{ \sum_{i=1}^{N} \left[\Delta + \sigma_i^2 (X_i' X_i)^{-1} \right]^{-1} \right\}^{-1} \left[\Delta + \sigma_i^2 (X_i' X_i)^{-1} \right]^{-1}, \\ \widehat{\beta} &= (X_i' X_i)^{-1} X_i' y_i. \end{aligned} \tag{18}$$

The variance of the estimator can be written as

$$\mathrm{Var}(\widehat{\beta}_{\mathrm{GLS}}) = \left(\sum_{i=1}^{N} X_i' \psi_i^{-1} X_i \right)^{-1} = \left\{ \sum_{i=1}^{N} \left[\Delta + \sigma_i^2 (X_i' X_i)^{-1} \right]^{-1} \right\}^{-1}. \tag{19}$$

Using $\widehat{\beta}_i = (X_i' X_i)^{-1} X_i' y_i$ and $\widehat{u}_i = y_i - X_i \widehat{\beta}_i$, we can obtain the unbiased estimator of σ_i^2 and Δ.

$$\begin{aligned} \sigma_i^2 &= \frac{\widehat{u}_i' u_i}{T - K} = \frac{1}{T - K} y_i' \left(I - X_i (X_i' X_i)^{-1} X_i' \right) y_i, \\ \widehat{\Delta} &= \frac{1}{N - 1} \sum_{i=1}^{N} \left(\widehat{\beta}_i - N^{-1} \sum_{i=1}^{N} \widehat{\beta}_i \right) \left(\widehat{\beta}_i - N^{-1} \sum_{i=1}^{N} \widehat{\beta}_i \right)' \\ &\quad - \frac{1}{N} \sum_{i=1}^{N} \widehat{\sigma}_i^2 (X_i' X_i)^{-1}. \end{aligned} \tag{20}$$

However, $\widehat{\Delta}$ obtained from estimator might be negative. In this case, we chose

$$\widehat{\Delta} = \frac{1}{N - 1} \sum_{i=1}^{N} \left(\widehat{\beta}_i - N^{-1} \sum_{i=1}^{N} \widehat{\beta}_i \right) \left(\widehat{\beta}_i - N^{-1} \sum_{i=1}^{N} \widehat{\beta}_i \right)'. \tag{21}$$

Thus, even though the estimator is not unbiased, it is invariable nonnegative. Moreover, when $T \longrightarrow \infty$, the estimate is consistent. Therefore, $\widehat{\beta}_{\mathrm{GLS}}$ obeys an asymptotic normal distribution and is a valid estimator of β.

Figure 1 presents the flowchart of the proposed synthetic model which integrates the finite element method into a random coefficient model based on the statistical model. The cross-section displacement data are analyzed as a panel in the random coefficient model, and the independent random coefficients ξ_i and ψ_i obey normal distributions. In addition, the proposed model can derivate the actual elastic modulus and actual coefficient of linear expansion at each monitoring point, which are dominant factors representing dam's properties.

3. Case Study

We selected the concrete dam at Jinping-I hydropower station as an example, which is the tallest arch dam in the world at present with a height of 305 m (the elevation of the dam crest is 1885 m and the elevation of dam foundation is 1580 m). It is a double-curved arch dam with the crest width

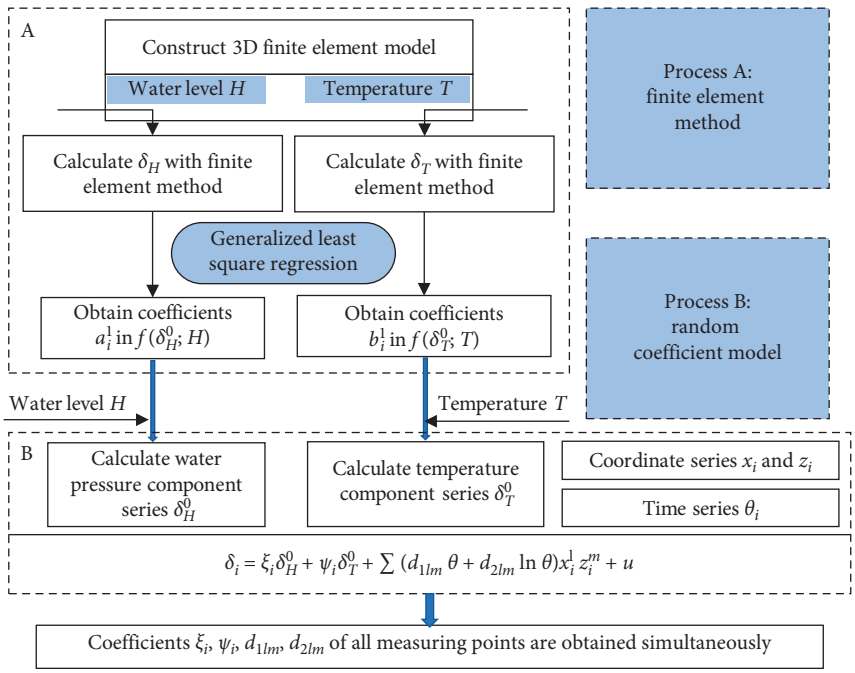

Figure 1: Flowchart of the proposed model which integrates the finite element method into a random coefficient model based on the statistical model.

of 16 m and the reservoir volume of $474 \times 10^6\ \mathrm{m}^3$. The dam is located in the southwest of China at the Yalong River (see Figure 2). The construction of the dam's body was completed on June 2013.

The displacement of an arch dam consists of three parts: vertical, tangential, and radial displacement, among which radial displacement is the most important indicator to evaluate the health of a concrete arch dam. Hence, we took the radial displacement as an example in this study. In order to monitor the radial displacement, the plumb system, consisting of 40 direct plumb meters and 30 reversed plumb meters, was installed in the selected dam. The structures of plumb meters are illustrated in Figure 3. For the direct plumb meter, the anchor is fitted on the dam crest with a block and, for the reversed plumb meter, the anchor is buried in the bedrock of dam foundation. The model of plumb meters used in this project is the CCD 50 manufactured by Xi'an Huateng Co., Ltd., with a measurement range of 0–0.1 m, a resolution of $0.1 \times 10^{-4}\ m$, and a measurement accuracy of $0.1 \times 10^{-3}\ m$.

In this study, we selected a dataset of 24 monitoring points that were recorded during the period from June 16, 2013, to August 25, 2015. There are 26 sections from left bank to right bank and 6 vertical lines (5#, 9#, 11#, 13#, 16#, and 19#) in the dam. The 24 monitoring points were located on the 6 indicated vertical lines (see Figure 4).

Since the dataset had been selected, we first eliminated the misdata and obtained 274 validated data samples for each monitoring point. As shown in Figure 5, the temperature evolution has a significant regular periodicity relative to time. The upstream water level is manually

Figure 2: Photograph of Jinping-I hydropower station.

controlled depending on the water resources allocation of the whole river basin. The water level in June 2013 was fairly low, as it was just newly constructed and putted into operation. Since then, the water level was gradually increased into a normal level.

Figure 6 shows the time evolution of the monitored radial displacement for all the monitoring points. We classified the monitoring points by their spatial distribution (i.e., the vertical lines where they are located). When coupled with the graphic information in Figures 5(a) and 6, it is notable that the general trend of the monitored radial displacement is approximately in line with the upstream water level. Another noticeable trend is the similarity in radial displacement for monitoring points at one vertical line and for adjacent monitoring points, which means that the displacement has a strong structural correlation.

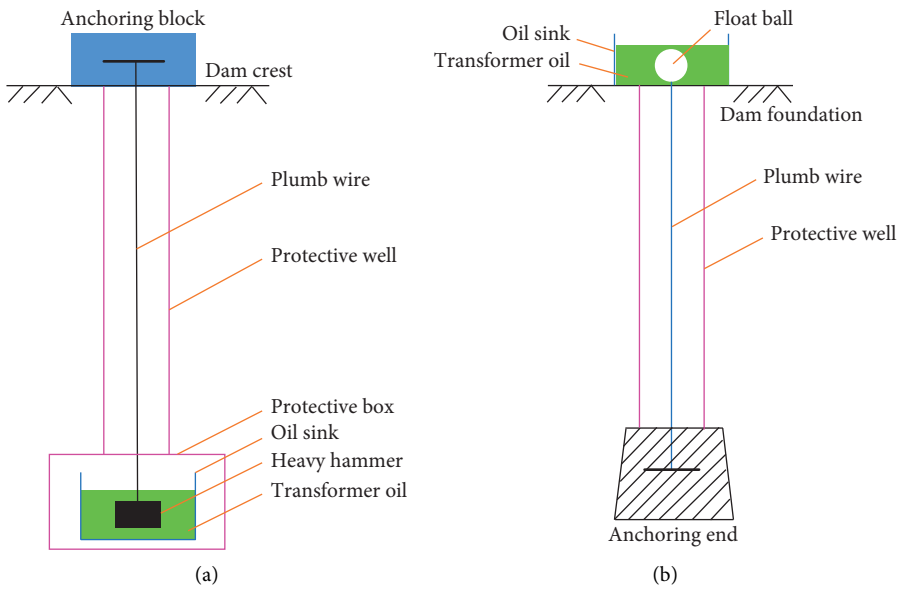

Figure 3: Plumb meters used in the selected concrete dam: (a) direct plumb and (b) reversed plumb [25].

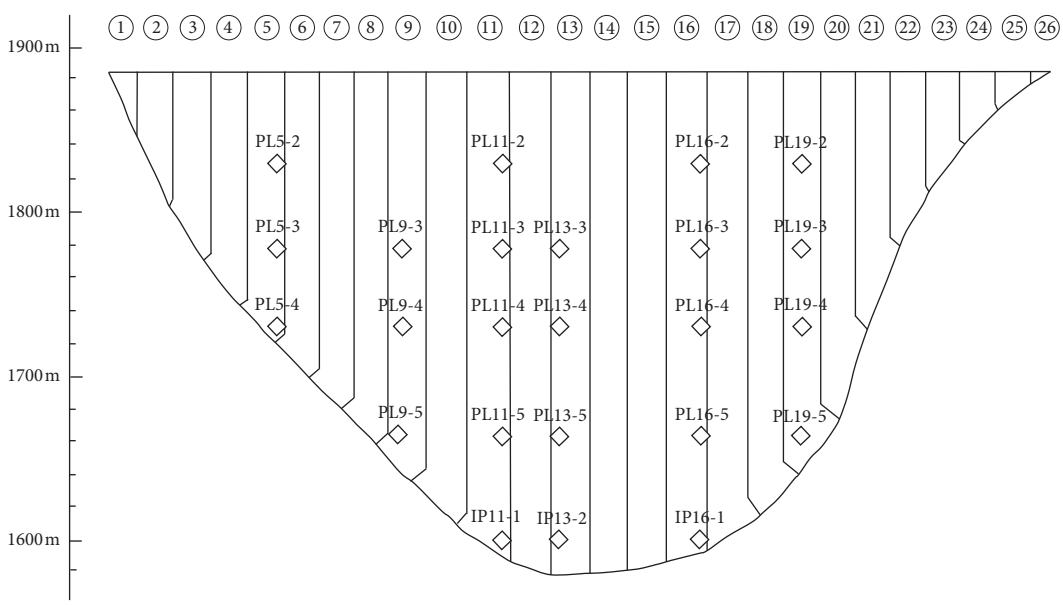

Figure 4: Distribution of dam sections and the monitoring points from the upstream side view.

4. Results

4.1. Coefficient Determination Using the Finite Element Model. In order to quantify the spatial distribution of displacement of all monitoring points, we first established a three-dimensional finite element model based on the actual geological characteristics of the dam (see Figure 7). The three-dimensional model includes three sections: dam body, dam foundation, and surrounded mountains; and the dam body was discretized into 38537 elements and 31941 nodes. The boundary of surrounding mountains was set to 2–3 times higher than the dam body in all the directions (x, y, and z). The model was constrained in the normal direction for all the lateral boundaries and was fixed in all directions for the bottom boundary; the crest of the dam and the dam body were free to move. The water load was merely applied to the upstream surface of dam and the bottom of reservoir; the elastic modulus of dam body and dam foundation were initially set to 30 GPa and 25 GPa, respectively.

4.1.1. Coefficients for Water Pressure Component. To shed light on the water pressure component acting on the dam displacement, we merely apply water load in this case. As the upstream water level of Jinping-I hydropower station varied from 1700 m to 1880 m during the selected period, here we

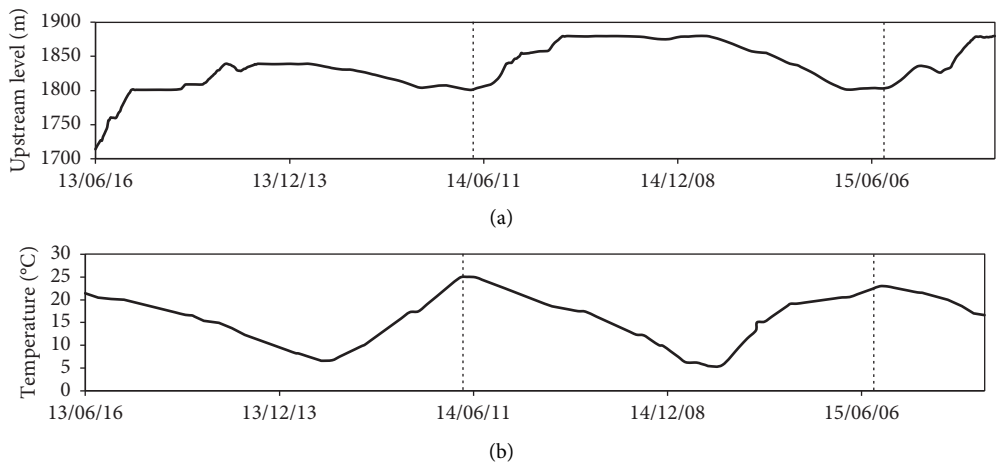

Figure 5: Time evolution of the (a) upstream level and (b) temperature.

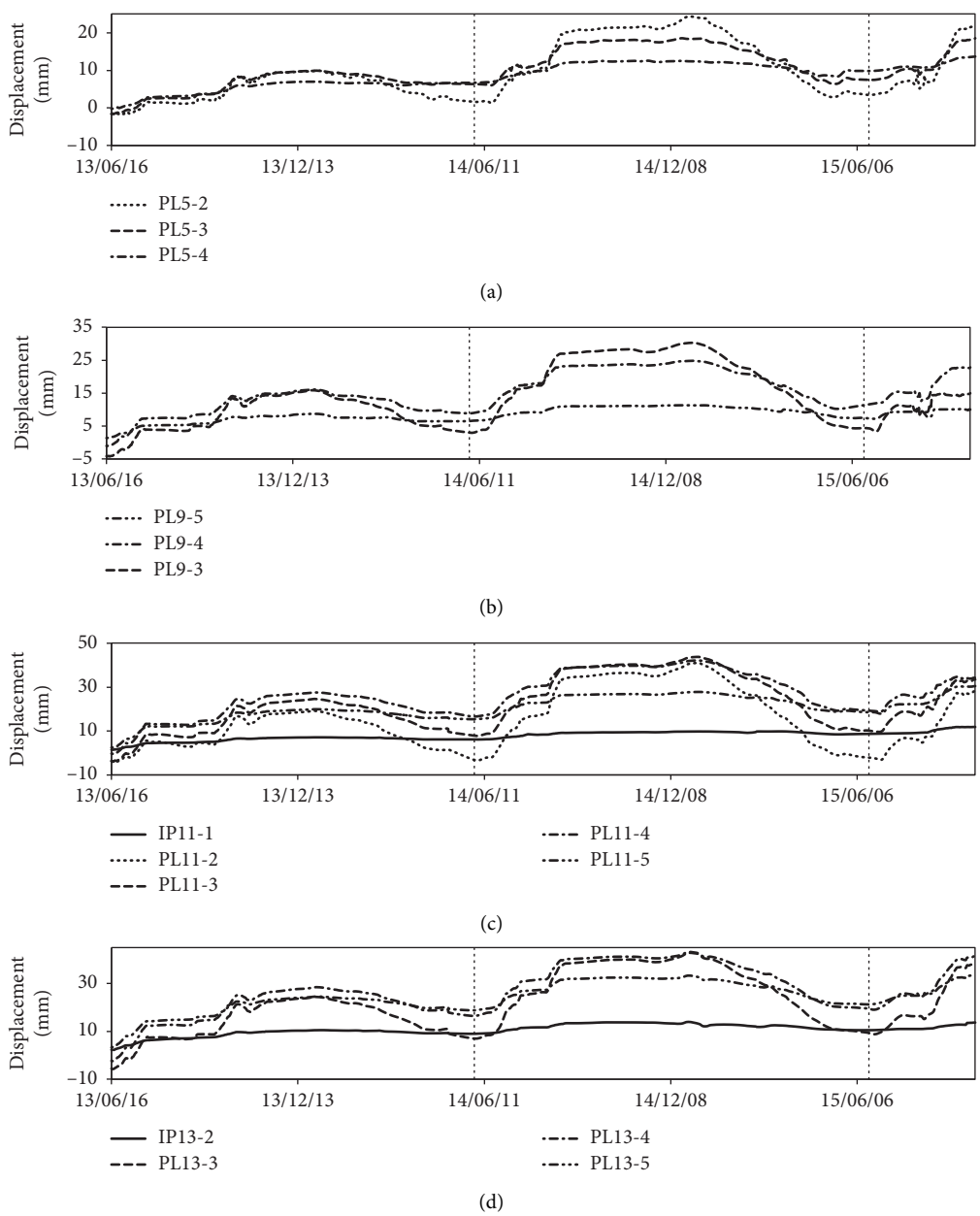

Figure 6: Continued.

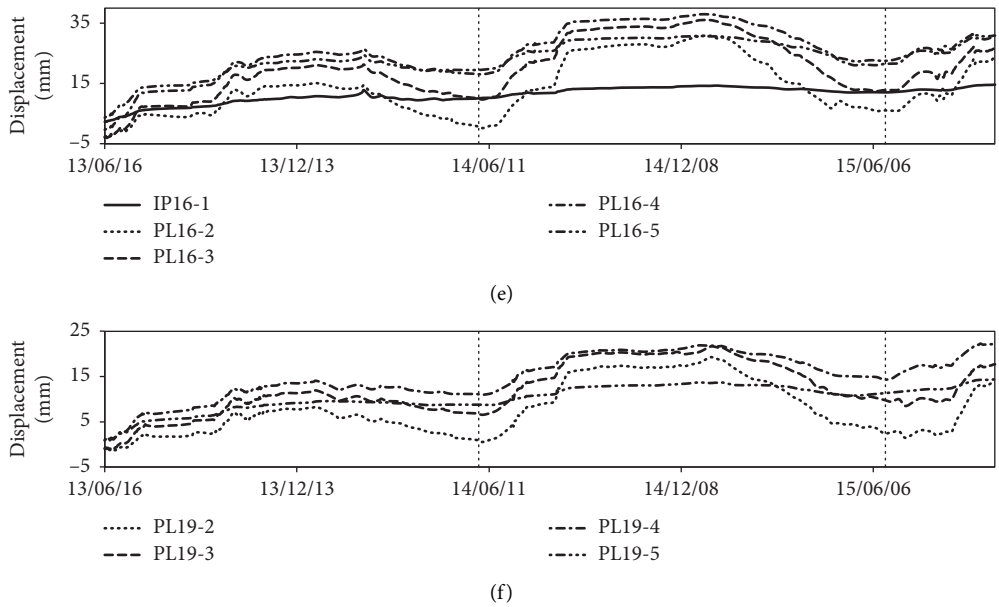

Figure 6: Time variation of the monitored radial displacement for monitoring points located at (a) vertical line 5#, (b) vertical line 9#, (c) vertical line 11#, (d) vertical line 13#, (e) vertical line 16#, and (f) vertical line 19#.

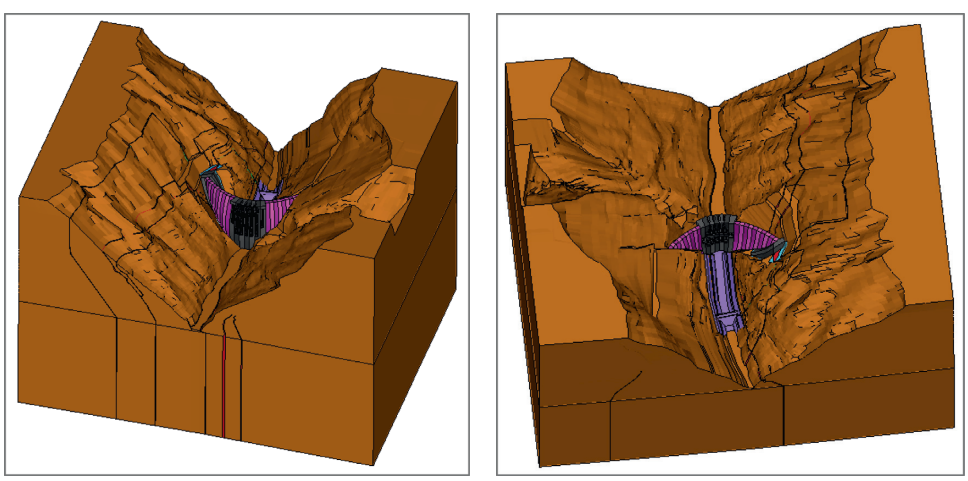

(a) (b)

Figure 7: Finite element model of the Jinping-I arch dam: (a) upstream side view and (b) downstream side view.

simulated the dam displacement under six water levels within this range, that is, 1700 m, 1740 m, 1780 m, 1820 m, 1860 m, and 1880 m.

Figure 8 exhibits the radial displacement simulated by the finite element method under three water levels (1700 m, 1780 m, and 1880 m). We can see that the displacements in all these subfigures are approximately horizontal symmetry, with the displacement at the midline being more significant than in border areas. In addition, with the increasing of upstream water level, the vertical coordinate of the center of minimum displacement region moves from the bottom to the dam crest.

After the radial displacement field on the cross section had been simulated, we can obtain the displacement at each monitoring point under the six selected upstream water levels. Simulated radial displacement of all the monitoring points versus upstream water level is illustrated in Figure 9. For all monitoring points, the radial displacement increased sharply with the increase of the upstream water level.

We then calculated the coefficients a_i^1 (introduced in equation (8) in Section 2) in the water pressure components by ordinary least square (OLS) regression based on simulated radial displacement. As an arch dam, $i = 1, 2, 3, 4$ The coefficients a_1^1, a_2^1, a_3^1, and a_4^1 for each monitoring point are listed in Table 1. The coefficients a_i^1 will be used in the statistical model solved by random coefficient model in Section 4.2.

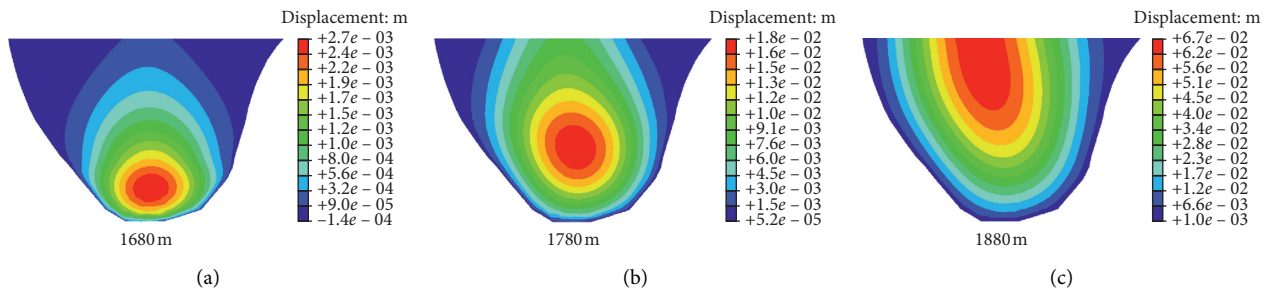

Figure 8: Radial displacement simulated by finite element method under varying upstream water levels: (a) 1700 m; (b) 1780 m; and (c) 1880 m.

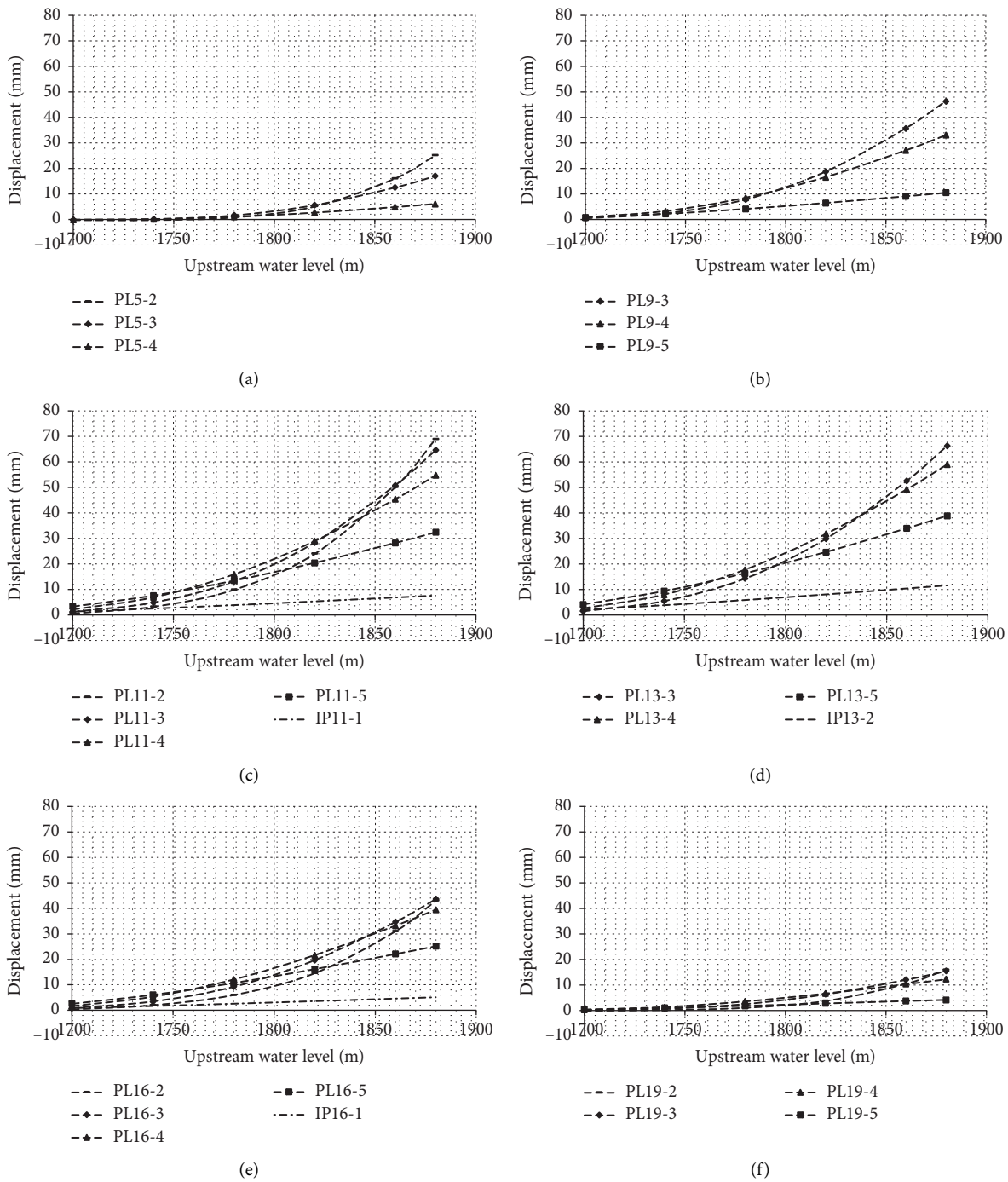

Figure 9: The radial displacement versus upstream water level simulated by finite element method for monitoring points located at vertical line: (a) 5#; (b) 9#; (c) 11#; (d) 13#; (e) 16#; and (f) 19#.

Table 1: Coefficients a_i^1 fitted by the simulation results of the finite element model.

Measuring points	a_4^1	a_3^1	a_2^1	a_1^1
PL5-2	$3.95E-09$	$-2.05E-05$	$3.54E-02$	$-2.04E+01$
PL5-3	$6.96E-10$	$-3.35E-06$	$5.35E-03$	$-2.83E+00$
PL5-4	$-1.95E-10$	$1.15E-06$	$-2.22E-03$	$1.41E+00$
PL9-3	$9.25E-10$	$-4.13E-06$	$6.01E-03$	$-2.84E+00$
PL9-4	$-6.41E-10$	$3.85E-06$	$-7.50E-03$	$4.79E+00$
PL9-5	$-2.51E-10$	$1.40E-06$	$-2.57E-03$	$1.56E+00$
PL11-2	$5.15E-09$	$-2.62E-05$	$4.46E-02$	$-2.53E+01$
PL11-3	$7.45E-10$	$-2.97E-06$	$3.65E-03$	$-1.28E+00$
PL11-4	$-1.01E-09$	$6.00E-06$	$-1.16E-02$	$7.35E+00$
PL11-5	$-5.47E-10$	$3.08E-06$	$-5.68E-03$	$3.44E+00$
IP11-1	$-8.74E-11$	$4.78E-07$	$-8.53E-04$	$4.99E-01$
PL13-3	$5.72E-10$	$-2.06E-06$	$2.05E-03$	$-3.54E-01$
PL13-4	$-1.12E-09$	$6.63E-06$	$-1.27E-02$	$8.03E+00$
PL13-5	$-6.33E-10$	$3.56E-06$	$-6.56E-03$	$3.97E+00$
IP13-2	$-1.21E-10$	$6.67E-07$	$-1.19E-03$	$6.99E-01$
PL16-2	$3.61E-09$	$-1.85E-05$	$3.15E-02$	$-1.79E+01$
PL16-3	$1.97E-10$	$-3.88E-07$	$-3.84E-04$	$8.05E-01$
PL16-4	$-1.03E-09$	$5.93E-06$	$-1.12E-02$	$6.92E+00$
PL16-5	$-4.84E-10$	$2.69E-06$	$-4.90E-03$	$2.95E+00$
IP16-1	$-6.23E-11$	$3.39E-07$	$-6.03E-04$	$3.51E-01$
PL19-2	$2.37E-09$	$-1.23E-05$	$2.13E-02$	$-1.23E+01$
PL19-3	$1.06E-10$	$-2.92E-07$	$6.88E-05$	$2.05E-01$
PL19-4	$-5.24E-10$	$2.94E-06$	$-5.43E-03$	$3.33E+00$
PL19-5	$-1.32E-10$	$7.17E-07$	$-1.28E-03$	$7.60E-01$

4.1.2. Coefficients for Temperature Component. Similar to the calculation of the coefficients in water pressure component, as the temperature of Jinping region varies from 4°C to 24°C in the real world, we selected six temperatures within this range: 4°C, 8°C, 12°C, 16°C, 20°C, and 24°C. We simulated the radial displacement under these temperatures using the finite element method and then obtained the relation between simulated radial displacement and indicated temperatures. As shown in Figure 10, in contrast with the water load impact, the radial displacement declines steadily with the rise in temperature.

Fitted with the simulation results, we obtained the coefficients b_i^1 ($i = 1$, (2) in equation (11) (see section 2.1) for each monitoring point. It should be noted that the displacement curves in Figure 10 never pass the origin of coordinate axes, which implies the necessity of adjusting equation (11) by adding a constant term. Table 2 shows the fitting results of the coefficients b_i^1 and the constant term.

4.2. Fitting Using the Random Coefficient Model. After the coefficients in the water pressure component and temperature component had been obtained, we fitted the monitoring data based on equation (13) using the random coefficient model.

The coefficients of the aging components d_{1lm} and d_{2lm} for each monitoring point were fitted by the random coefficient model (see Table 3). Meanwhile, we can obtain the ratio between design and actual elastic modulus ξ and the ratio between actual and design coefficient of linear expansion ψ; then we can derive the actual elastic modulus E_c and actual coefficient of linear expansion α_c (see Table 4). The elastic modulus reflects the ability of being deformed elastically when a stress is applied on an object. The coefficient of linear expansion represents the capacity of the length changes when material is heated or cooled; namely, the length changes by an amount proportional to the original length and the change in temperature. The elastic modulus may serve to evaluate the dam's running status from the view of material.

It is interesting from Table 4 that E_c is dependent on the spatial location of monitoring points, where the minimum is 14.89 GPa at the monitoring point PL9-3, and the maximum is 32.51 GPa at IP16-1. We will provide a detailed discussion in section 5.2.

With the random coefficient model, the radial displacement of all the monitoring points can be modeled simultaneously. The datasets were divided into two groups; 80% of the whole data were selected as fitting data, and the other 20% were selected to validate the model (validation data). We developed the prediction model with the fitting data. Then, we used the validation data to evaluate the performance of the model. Taking the monitoring points located at vertical line 5# as an example, the fitting and predicting results obtained from the synthetic model are shown in Figure 11. Both the fitting results (left side of the line) and validating results (right side of the line) fit well with the monitored data.

In order to validate the synthetic model, we calculated the correlation coefficient R and the residual standard deviation s for the data series of all the monitoring points. The expressions of R and s are presented as follows:

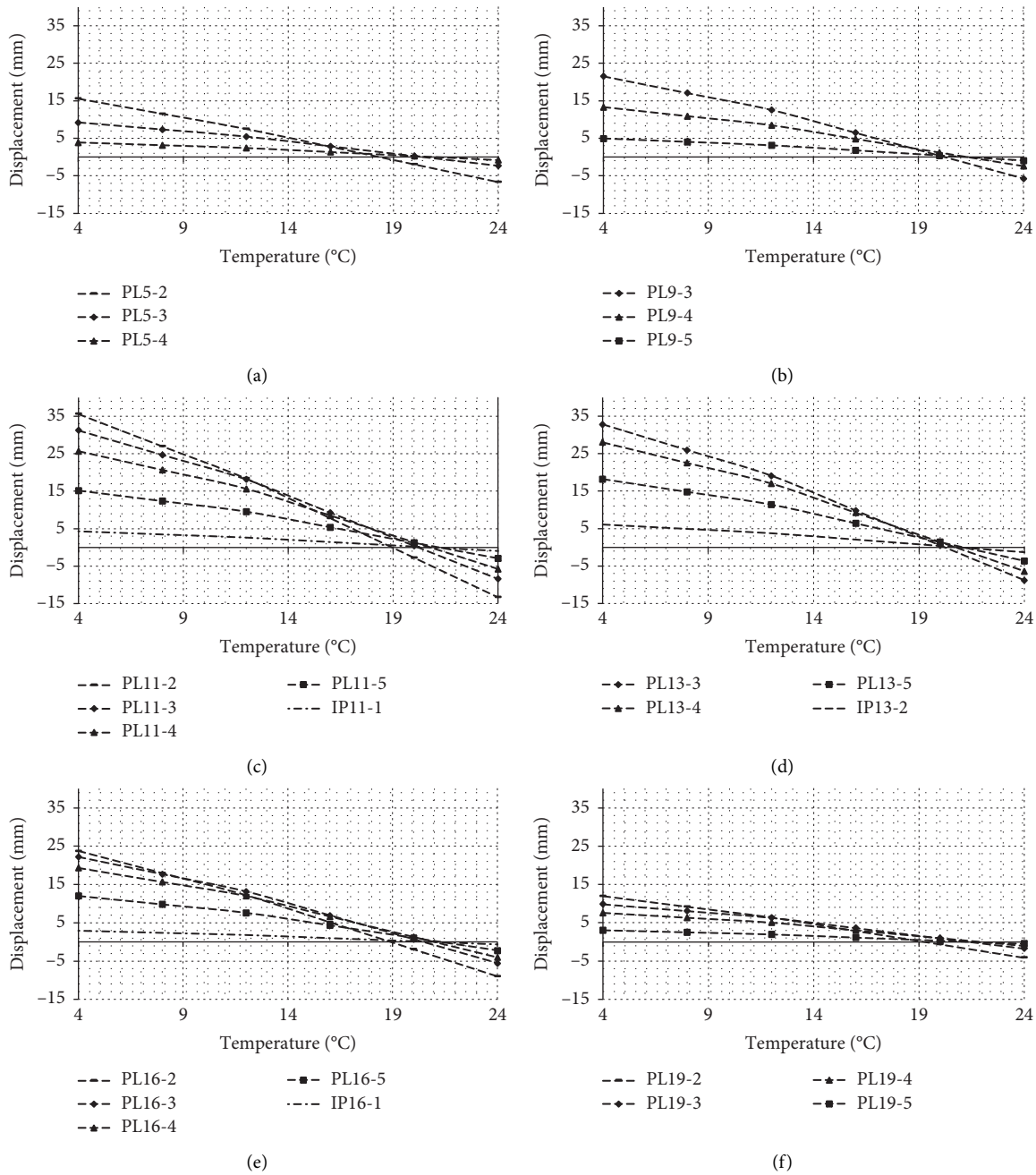

Figure 10: Variation of the radial displacement with external temperature simulated by finite element method for monitoring points located at vertical line: (a) 5#; (b) 9#; (c) 11#; (d) 13#; (e) 16#; and (f) 19#.

$$R = \sqrt{\frac{\sum_{i=1}^{n} \left(\widehat{y}_i - \overline{y}_i\right)^2}{\sum_{i=1}^{n} \left(y_i - \overline{y}_i\right)^2}},$$
$$s = \sqrt{\frac{\sum_{i=1}^{n} \left(\widehat{y}_i - \overline{y}_i\right)^2}{n-1}}. \tag{22}$$

Usually, a model can be validated once the correlation coefficient R is above 0.9. As exhibited in Table 5, R for all the monitored points are higher than 0.987, which means that the fitting results and the monitoring data have a quite good agreement. The residual standard deviation s is located in the range of 0.186 to 1.550. The data lead us to the conclusion that the model performed well in fitting radial displacement of concrete dam.

5. Discussion

5.1. Improvement of Prediction Precision. Here, we selected correlation coefficients R as the indicator to evaluate the prediction accuracy of proposed model and two previous models. One is the most commonly used statistical model based on ordinary least squares (OLS) regression. Another

Table 2: Coefficients b_i^1 and the constant term fitted by simulation results of the finite element model.

Measuring points	b_2^1	b_1^1	Constant term
PL5-2	−0.00691	$-9.24E-01$	19.3949
PL5-3	−0.00715	$-3.83E-01$	10.8835
PL5-4	−0.00333	$-1.43E-01$	4.50277
PL9-3	−0.01623	$-9.22E-01$	25.5644
PL9-4	−0.0121	$-4.57E-01$	15.3685
PL9-5	−0.0044	$-1.73E-01$	5.70124
PL11-2	−0.0196	$-1.91E+00$	43.6112
PL11-3	−0.0233	$-1.35E+00$	37.0455
PL11-4	−0.02127	$-9.91E-01$	30.0274
PL11-5	−0.01347	$-5.38E-01$	17.5743
IP11-1	−0.00356	$-1.66E-01$	5.02897
PL13-3	−0.02454	$-1.41E+00$	38.9179
PL13-4	−0.0231	$-1.09E+00$	32.817
PL13-5	−0.01599	$-6.55E-01$	21.119
IP13-2	−0.0052	$-2.25E-01$	7.0605
PL16-2	−0.01288	$-1.28E+00$	29.1189
PL16-3	−0.0174	$-9.13E-01$	26.1968
PL16-4	−0.01677	$-7.10E-01$	22.5246
PL16-5	−0.01088	$-4.17E-01$	13.919
IP16-1	−0.00255	$-1.08E-01$	3.42312
PL19-2	−0.00712	$-6.07E-01$	14.4608
PL19-3	−0.00903	$-3.30E-01$	11.2959
PL19-4	−0.0075	$-2.27E-01$	8.62348
PL19-5	−0.00276	$-1.01E-01$	3.44706

Table 3: The coefficients d_{1lm} and d_{2lm} in the aging component.

Measuring points	d_{1lm}	d_{2lm}
PL5-2	3.87	−0.17
PL5-3	2.73	5.62
PL5-4	4.84	4.67
PL9-3	−5.95	12.19
PL9-4	1.85	5.25
PL9-5	0.51	4.83
PL11-2	−2.00	−5.57
PL11-3	0.28	6.84
PL11-4	0.30	14.40
PL11-5	7.23	3.15
IP11-1	4.68	0.74
PL13-3	1.53	3.17
PL13-4	2.94	10.39
PL13-5	3.18	9.43
IP13-2	0.69	6.40
PL16-2	3.44	−0.50
PL16-3	−1.04	13.92
PL16-4	−0.43	20.68
PL16-5	3.75	12.28
IP16-1	2.92	7.33
PL19-2	−1.49	3.37
PL19-3	0.62	7.76
PL19-4	6.19	5.55
PL19-5	4.18	5.65

model was a random coefficient model improved by a clustering model named Gaussian mixture model (Clustering-RCM), because recent researches used clustering models to classify the monitoring points into several classes for the sake of considering the structural correlations among monitoring points. As introduced in Section 1, with only two explanatory variables, finite element method can simulate the water pressure component and temperature component of all monitoring points. In addition, synthetic model provides constraints for each monitoring point, whereas the clustering model merely provides constraint for each class; the number of explanatory variables in the proposed model is reduced more. Hence, the results of coefficients estimates are more stable and the prediction ability is better in the proposed model.

Table 4: The actual elastic modulus E_c and actual coefficient of linear expansion α_c at each monitoring point.

Monitoring points	E_c (GPa)	α_c (m)
IP11-1	23.64	$1.61E-06$
IP13-2	20.10	$1.08E-06$
IP16-1	32.51	$3.02E-06$
PL19-5	21.00	$3.41E-06$
PL19-4	20.70	$1.53E-06$
PL19-3	20.10	$2.12E-06$
PL19-2	19.50	$2.80E-06$
PL16-5	21.41	$1.39E-06$
PL16-4	16.60	$1.79E-06$
PL16-3	17.13	$2.37E-06$
PL16-2	16.23	$3.04E-06$
PL13-5	18.30	$1.03E-06$
PL13-4	18.11	$1.50E-06$
PL13-3	18.32	$2.03E-06$
PL11-5	19.25	$1.12E-06$
PL11-4	16.27	$1.64E-06$
PL11-3	16.87	$2.19E-06$
PL11-2	17.18	$2.63E-06$
PL9-5	17.89	$1.54E-06$
PL9-4	17.86	$1.87E-06$
PL9-3	14.89	$2.27E-06$
PL5-4	30.67	$3.46E-07$
PL5-3	23.00	$1.97E-06$
PL5-2	21.79	$2.91E-06$

As shown in Figure 12, the correlation coefficients R of three models based on validation dataset of 24 monitoring points are compared; the proposed model had the highest R in 14 monitoring points and Clustering-RCM model had the highest R in 7 monitoring points. For IP16-1, PL19-3, PL5-2, and PL16-2, the difference of R between the proposed model and Clustering-RCM model is smaller than 0.001. In summary, the proposed model has a better prediction precision than the Clustering-RCM model, and the Clustering-RCM model performs better than OLS regression.

5.2. Back-Analysis of Elastic Modulus. From the actual elastic modulus E_c at each monitoring point presented in Table 4, we can derive the field distribution of E_c for the whole dam section using a Lagrange polynomial interpolation (see Figures 13(a) and 13(b)). It is striking that the actual elastic modulus at one point is strongly dependent on its spatial location on the dam section. In particular, the actual elastic modulus is small in the central area and large in the border area.

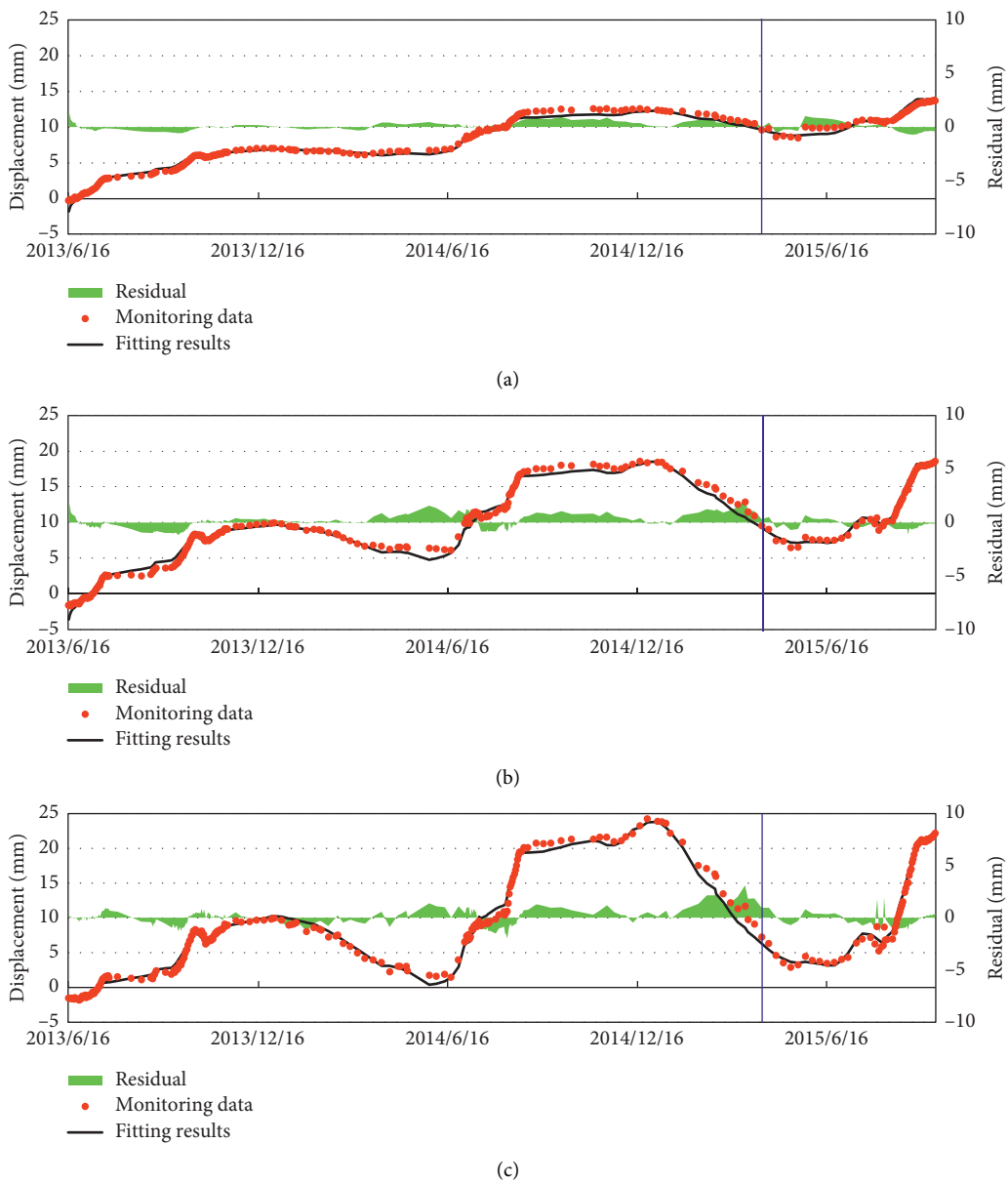

Figure 11: Modeling results for monitoring points located at vertical line 5#: (a) PL5-4, (b) PL5-3, and (c) PL5-2.

Elastic modulus is a variable material property during the running status owing to the external environments and time. It is usually obtained by back-calculation based on monitored displacement and corresponding upstream water level, which is roughly written as $E_c = (f(H)/\delta_H)$, where $f(H)$ is the expression of upstream water level. One reason for the regularity of elastic modulus distribution is that the displacement δ_H near foundation is limited owing to the strong restraint of dam foundation. Taking the annual radial displacement in 2014 as an example, the displacement in the central area is also higher than in border area (see Figure 13(c)). Hence, the elastic modulus of concrete used in the region of surrounding the dam foundation is higher than the dam center.

In Figure 13(d), the design elastic modulus of three divided region areas A, B, and C is 24 GPa, 23.5 GPa, and 23 GPa, respectively. First, it is noted that the actual elastic modulus for most areas on the dam has a deviation from the design value. Moreover, the actual elastic modulus in central areas is commonly smaller than the design value, whereas the values near the foundation are larger than design value. It is inevitable that each material may have different disintegration rate under the external load. Mainly, the distribution of residual between the actual and design elastic modulus roughly agrees with the spatial location and deformation under external load.

5.3. Limitations. The proposed method can be merely applied in projects with known topography data and design data which include material parameters of dam, dam foundation and mountains, and physical dimension.

Table 5: Correlation coefficient R and residual standard deviation s of the synthetic model for each monitoring point.

Measuring points	R (/)	S (mm)
IP11-1	0.999	0.256
IP13-2	0.994	0.360
IP16-1	0.991	0.287
PL19-5	0.997	0.528
PL19-4	0.993	0.186
PL19-3	0.999	0.234
PL19-2	0.998	0.445
PL16-5	0.992	0.893
PL16-4	0.993	0.873
PL16-3	0.998	0.514
PL16-2	0.987	0.270
PL13-5	0.985	0.292
PL13-4	0.998	0.281
PL13-3	0.988	0.231
PL11-5	0.987	0.488
PL11-4	0.993	0.223
PL11-3	0.999	1.550
PL11-2	0.994	0.581
PL9-5	0.998	0.365
PL9-4	0.995	0.363
PL9-3	0.990	0.283
PL5-4	0.992	1.223
PL5-3	0.987	0.473
PL5-2	0.997	1.410

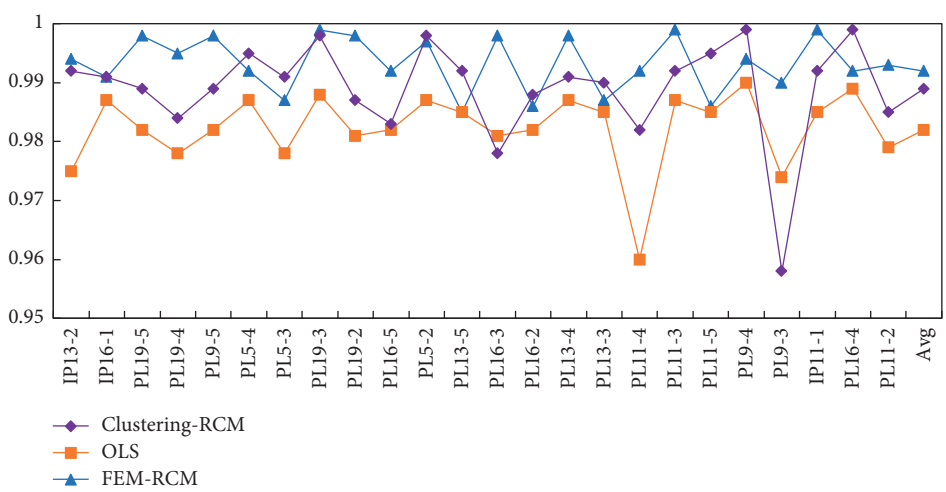

Figure 12: Comparing the correlation coefficient R of the FEM-RCM model with the clustering-RCM model and statistical model using OLS regression.

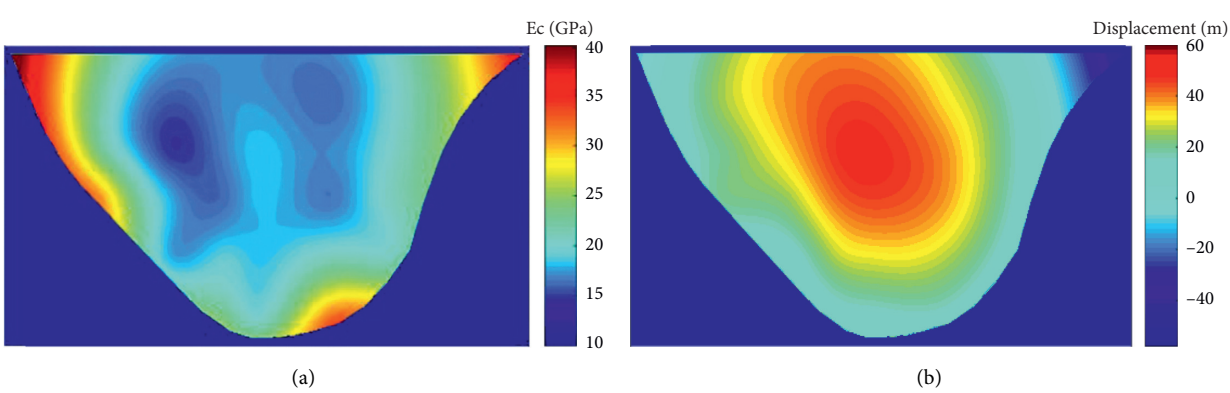

Figure 13: Continued.

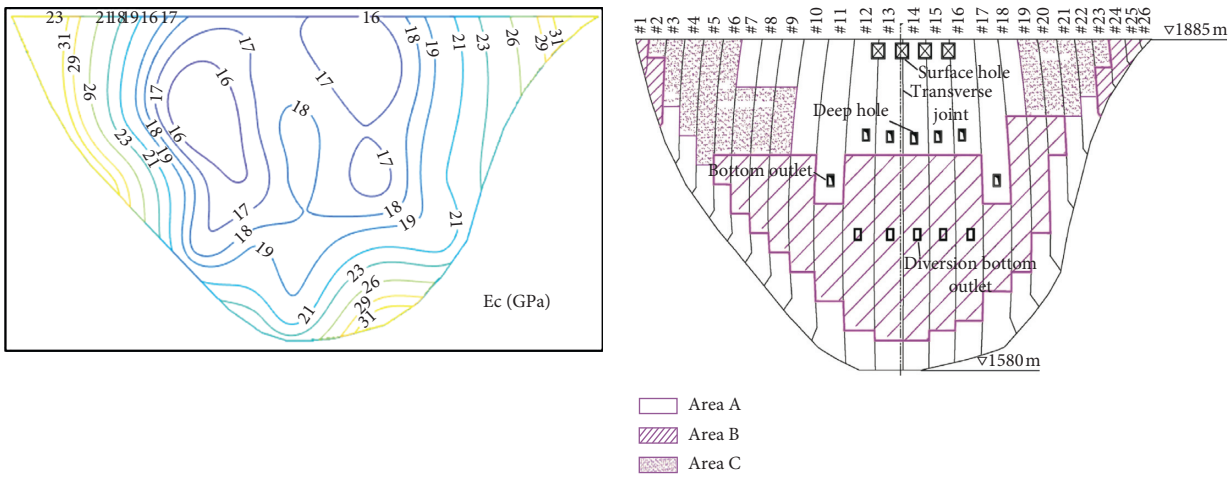

(c) (d)

Figure 13: The maps of (a) field distribution of actual elastic modulus E_c, (b) actual elastic modulus E_c, (c) annual radial displacement in 2014, and (d) zoning designation of concrete material [26].

Another issue that should be noticed is that the correctness of data at all monitoring points should be guaranteed. With random coefficient model, all data series are analyzed simultaneously, so the measurement errors in one monitoring point may affect the accuracy of other monitoring points.

6. Conclusions

In this article, we presented a synthetic model that integrates the finite element method into a random coefficient model. The primary objective is to take the structural correlations among each monitoring point into account in a statistical model.

With this objective in mind, we first used the finite element method to simulate the water pressure component and temperature component of displacement at each monitoring point, so as to constrain the spatial correlations among monitoring points. Then, with random coefficient method, explanatory variable coefficients of all monitoring points are calculated, obeying an asymptotic normal distribution. Finally, we selected the concrete arch dam in Jinping-I hydropower station as an example to validate the proposed model. Remarkable results can be concluded in two aspects.

First, with the proposed model, the modeling displacement data fitted well with the monitored data. We find that the proposed model performed better than a combined model of random coefficient model and Gaussian mixture clustering model, owing to the fact that finite element model can provide more rigorous constraints than clustering methods for each monitoring point.

Second, using a Lagrange interpolation, we can obtain the distribution field of the actual elastic modulus based on the actual elastic modulus at each monitoring point. The field distribution of the actual elastic modulus has deviation from the design value due to a coeffect of external load. In addition, with the help of finite element method, the distribution field of the displacement on the basis of monitored data can also be obtained.

Data Availability

The data used to support the findings of this study are available from the corresponding author upon request.

Conflicts of Interest

The authors declare that they have no conflicts of interest.

Acknowledgments

This work was supported by the National Key R&D Program of China (Grant no. 2016YFC0401908), National Natural Science Foundation of China (Grants nos. 51739003, 51579085, 51779086, 51579086, 51379068, 51579083, and 51609074), the Fundamental Research Funds for the Central Universities (2018B619X14), project funded by the Priority Academic Program Development of Jiangsu Higher Education Institutions (YS11001), Postgraduate Research & Practice Innovation Program of Jiangsu Province (KYCX18_0588), Special Project Funded by National Key Laboratory (20165042112), and Key R&D Program of Guangxi (AB17195074).

References

[1] Z. Wu, *Safety Monitoring Theory and its Application of Hydraulic Structures*, Higher Education, Beijing, China, 2003.

[2] S. Ahmad, B. M. Irons, and O. C. Zienkiewicz, "Analysis of thick and thin shell structures by curved finite elements," *International Journal for Numerical Methods in Engineering*, vol. 2, no. 3, pp. 419–451, 1970.

[3] P. Léger, P. Côté, and R. Tinawi, "Finite element analysis of concrete swelling due to alkali-aggregate reactions in dams," *Computers & Structures*, vol. 60, no. 4, pp. 601–611, 1996.

[4] P. Bukenya, P. Moyo, H. Beushausen, and C. Oosthuizen, "Health monitoring of concrete dams: a literature review," *Journal of Civil Structural Health Monitoring*, vol. 4, no. 4, pp. 235–244, 2014.

[5] V. Ranković, N. Grujović, D. Divac, and N. Milivojević, "Development of support vector regression identification model for prediction of dam structural behaviour," *Structural Safety*, vol. 48, pp. 33–39, 2014.

[6] A. Penman and A. Charles, "Constructional deformations in rockfill dam," *Journal of Soil Mechanics & Foundations Div*, vol. 99, 1973.

[7] L. Cheng, Y. R. Liu, Q. Yang, Y. W. Pan, and Z. Lv, "Mechanism and numerical simulation of reservoir slope deformation during impounding of high arch dams based on nonlinear FEM," *Computers and Geotechnics*, vol. 81, pp. 143–154, 2017.

[8] M. Alembagheri and R. Sheikhzadeh Shayan, "Seismic performance evaluation of concrete arch-gravity dams using incremental dynamic analysis," *Modares Civil Engineering Journal*, vol. 18, pp. 155–167, 2019.

[9] M. Abraham, N. S. Mani, A. Mathew, D. I. Gopinath, and A. Balan, "Dynamic study and analysis of gravity dam considering foundation interaction effect and sloshing effect," in *Green Buildings and Sustainable Engineering*, pp. 267–280, Springer, Berlin, Germany, 2019.

[10] A. Seghir, A. Tahakourt, and G. Bonnet, "Coupling FEM and symmetric BEM for dynamic interaction of dam-reservoir systems," *Engineering Analysis with Boundary Elements*, vol. 33, no. 10, pp. 1201–1210, 2009.

[11] W. F. Caspary, W. Haen, and H. Borutta, "Deformation analysis by statistical methods," *Technometrics*, vol. 32, no. 1, pp. 49–57, 1990.

[12] B. Liu, B. Zhang, J. Yu, and G. Gu, "Forecast for dam deformation based on multiple linear regression model," *Yangtze River*, vol. 20, p. 017, 2010.

[13] B. Stojanovic, M. Milivojevic, M. Ivanovic, N. Milivojevic, and D. Divac, "Adaptive system for dam behavior modeling based on linear regression and genetic algorithms," *Advances in Engineering Software*, vol. 65, pp. 182–190, 2013.

[14] A. Jiang and X. Feng, "Case-based SVM method for maximal deformation forecasting of surrounding rocks of tunnels," *Journal of Northeastern University (Natural Science)*, vol. 25, pp. 793–795, 2004.

[15] S. Mahani, S. Shojaee, E. Salajegheh, and M. Khatibinia, "Hybridizing two-stage meta-heuristic optimization model with weighted least squares support vector machine for optimal shape of double-arch dams," *Applied Soft Computing*, vol. 27, pp. 205–218, 2015.

[16] B. Stojanovic, M. Milivojevic, N. Milivojevic, and D. Antonijevic, "A self-tuning system for dam behavior modeling based on evolving artificial neural networks," *Advances in Engineering Software*, vol. 97, pp. 85–95, 2016.

[17] S. Demirkaya, "Deformation analysis of an arch dam using ANFIS," in *Proceedings of the Second International Workshop on Application of Artificial Intelligence and Innovations in Engineering Geodesy*, pp. 21–31, Braunschweig, Germany, 2010.

[18] H. Su, X. Li, B. Yang, and Z. Wen, "Wavelet support vector machine-based prediction model of dam deformation," *Mechanical Systems and Signal Processing*, vol. 110, pp. 412–427, 2018.

[19] J. Valença and E. Júlio, "MCrack-Dam: the scale-up of a method to assess cracks on concrete dams by image processing. The case study of Itaipu Dam, at the Brazil-Paraguay border," *Journal of Civil Structural Health Monitoring*, vol. 8, no. 5, pp. 857–866, 2018.

[20] L. Fumin, "Application of Kalman filter method in dam deformation analysis," *Site Investigation Science and Technology*, vol. 1, pp. 43–45, 2002.

[21] C. Shao, C. Gu, M. Yang, Y. Xu, and H. Su, "A novel model of dam displacement based on panel data," *Structural Control and Health Monitoring*, vol. 25, Article ID e2037, 2018.

[22] Y. Hu, C. Shao, C. Gu, and Z. Meng, "Concrete dam displacement prediction based on an ISODATA-GMM clustering and random coefficient model," *Water*, vol. 11, no. 4, p. 714, 2019.

[23] P. Léger and M. Leclerc, "Hydrostatic, temperature, time-displacement model for concrete dams," *Journal of Engineering Mechanics*, vol. 133, no. 3, pp. 267–277, 2007.

[24] P. A. Swamy, "Efficient inference in a random coefficient regression model," *Econometrica: Journal of the Econometric Society*, vol. 38, pp. 311–323, 1970.

[25] D. Bo, T. Hu, Z. Huang, and C. Fang, "A spatio-temporal clustering and diagnosis method for concrete arch dams using deformation monitoring data," *Structural Health Monitoring*, vol. 18, pp. 1355–1371, 2019.

[26] S.-y. Wu, W. Cao, and J. Zheng, "Analysis of working behavior of Jinping-I Arch Dam during initial impoundment," *Water Science and Engineering*, vol. 9, no. 3, pp. 240–248, 2016.